INTRA-RETINAL LAYER SEGMENTATION OF OPTICAL COHERENCE TOMOGRAPHY USING DIFFUSION MAP

Raheleh Kafieh[1], Hossein Rabbani[1,2], Michael Abramoff[2], Milan Sonka[2]

[1] Biomedical Engineering Dept., Medical Image & Signal Processing Research Center, Isfahan Univ. of Medical Sciences, Isfahan, Iran
[2]The Iowa Institute for Biomedical Imaging, The University of Iowa
Email: hossein-rabbani@uiowa.edu

ABSTRACT

Optical coherence tomography (OCT) is known to be one of the powerful and noninvasive methods in retinal imaging. OCT uses retroreflected light to provide micron-resolution, cross-sectional scans of biological tissues. In contrast to OCT technology development, which has been a field of active research since 1991, OCT image segmentation has only been fully explored during the last decade. In this paper, we introduce a fast segmentation method based on a new kind of spectral graph theory named diffusion maps. The research is performed on spectral domain OCT images depicting normal macular appearance. In contrast to our recent methods of graph based OCT image segmentation, the presented approach does not require edge-based image information and rather relies on regional image texture. Consequently, the proposed method demonstrates robustness in situations of low image contrast or poor layer-to-layer image gradients. This method is tested on thirteen 3D macular SD-OCT images obtained from eyes without pathologies with Topcon 3D OCT-1000 imaging system (with a size of 650 × 512 × 128 voxels and a voxel resolution of 4.81 × 13.67 × 24.41 μm^3). The mean unsigned and signed border positioning errors (mean ± SD) was 8.52±3.13 and -4.61±3.35 micrometers, respectively. The average computation time of the proposed algorithms (implemented with MATLAB) was 12 seconds per 2D slice.

Index Terms— Optical coherence tomography (OCT), segmentation, spectral graph theory, diffusion map.

1. INTRODUCTION

Optical coherence tomography (OCT) is a powerful imaging modality used to image various aspects of biological tissues, such as structural information, blood flow, elastic parameters, change of polarization states, and molecular content [1]. OCT uses the principle of low coherence interferometry to generate two- or three-dimensional imaging of biological samples by obtaining high-resolution cross-sectional backscattering profiles (figure 1.a). Two kinds of OCT (time-domain and frequency-domain (SD-OCT)) are available in retinal analysis. In contrast to OCT technology development which has been a field of active research since 1991, OCT image segmentation has only been more fully explored during the last decade. Segmentation, however, remains one of the most difficult and at the same time most commonly required step in OCT image analysis. No typical segmentation method exists that can be expected to work equally well for all tasks [2]. We may classify the OCT segmentation approaches into five distinct groups according to the image domain subjected to the segmentation algorithm. Let's define 5 separate families of segmentation approaches: Methods applicable to A-scan, B-scan, active contour approaches (frequently in 2-D), analysis methods utilizing artificial intelligence, and segmentation methods using 3D graphs constructed from the 3D OCT volumetric images. To have a fair comparison between the time complexities of these methods, it should be mentioned that the CPU used in the methods have relatively similar speeds.

A-scan methods were firstly introduced by Hee [3] and were popular until 2005[4-5]. They completely lacked the contribution from 3D image context and suffered from excessive computation time and lack of layer detection accuracy.

B-Scan methods allowed to deal with 2D noise by incorporating better denoising algorithms during the preprocessing step. However, the dependency of these algorithms on noise reduction required very complicated and time-consuming denoising like anisotropic diffusion, which made these algorithms too weak from the speed point of view [6-7]. Additionally, the underlying intensity based methods and the relevant threshold selection was a difficult problem that was case-dependent.

Active contours approaches to OCT image segmentation were first proposed by Cabrera Fernández [8] and modified by Yazdanpanah [9]. Unfortunately the time complexity and exact error reports are not available in any of the mentioned papers, which makes such methods difficult to compare with other published methods. Regardless, active contour algorithms surpass the performance of intensity based B-Scan approaches, both in resistance to 2D noise and in accuracy.

Artificial intelligence based approaches were presented in [10, 11] and relied on a multiresolution hierarchical support vector machine (SVM) or on fuzzy C-means clustering techniques. The first one reported to have low ability in detection (6pixels of line difference and 68% of thickness difference) and a high time complexity (2 minutes). But, the latter [11] reported to have better results by only 2 pixels of linear difference and 45 seconds of time complexity. Overall, these methods cannot be categorized as established standard approaches since later-introduced methods like graph-based approaches can surpass them both in accuracy and time complexity.

3D graph-based methods seem so far to be best suited for the task in comparison to the above-mentioned approaches. Their time requirements can be reduced to about 45 seconds per 3D volume (480x512x128 voxels) and they routinely achieve high accuracy with about 2.8μm of layer-surface segmentation error. Such methods take advantage of newly developed 3D imaging systems, which provide better visualization and 3D rendering of segmentation results [12-14]. By design benefitting from contextual information represented in the analysis graph, these methods are robust to noise and do not require advanced noise reduction in the preprocessing steps. While there is no theoretical limit on the number of layers that can be simultaneously segmented by these approaches, up to 10 layers are routinely identified in retinal OCT images, performance that unavailable to the other above-referenced algorithms.

One of the most promising methods among the studied strategies is graph based image segmentation. We focus on novel spectral- geometric methods for graph based image [15-18] and explore a two step diffusion map approach to segmentation of OCT images. The proposed method is obviously categorized in 3D graph based methods; to clear up, we should focus on partitioning methods proposed on graphs. Similar to signal processing approaches, most of graph based partitioning methods were based on time-domain analysis. It means that the graph partitioning was usually based on properties in the graph domain like gradient or texture. But newly developed methods in frequency domain are based on signal analysis in new domains (similar to Fourier transform in signal processing). The proposed Diffusion Map method is similarly working on Fourier transform applied on graphs and the method can utilize the intrinsic capabilities of the frequency space consequently.

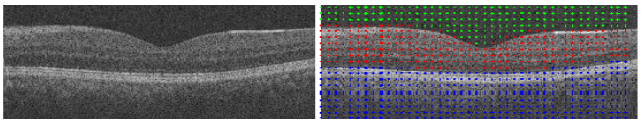

Figure.1. a) A sample OCT image. b) Results of the first diffusion map.

2. DIFFUSION MAPS

Diffusion maps [19] are a spectral embedding of a set X of n nodes, for which local geometries are defined by a kernel k: X × X → R. The kernel k satisfies k(x,y) ≥ 0, and k(x,y)=k(y,x). This kernel can be interpreted as an affinity between nodes. The resulting graph (an edge between x and y carries the weights k(x,y)) can be transformed into a reversible Markov chain by the so called normalized graph Laplacian construction. We define a row normalized version of $k(x,y)$, called $p(x,y)$ (new kernel):

$$s(x) = \sum_y k(x,y) \quad (1)$$

and

$$p(x,y) = \frac{k(x,y)}{s(x)} \quad (2)$$

This new kernel is no longer symmetric, but it satisfies

$$\forall x,\ \sum_y p(x,y) = 1 \quad (3)$$

Therefore it can be interpreted as the probability of the transition from node x to node y in one time step, or a transition kernel of a Markov chain. P is the Markov matrix whose elements are $p(x,y)$ and the elements of its powers P^τ are the probability of the transition from node x to node y in τ time steps. The operator P defines a geometry which can be mapped to an Euclidean geometry by an eigenvalue decomposition of P.

The latter results in a sequence of eigenvalues $\lambda_1, \lambda_2 \ldots$ and corresponding eigenfunctions $\Psi_1, \Psi_2, \ldots$ that fulfill $P\Psi_i = \lambda_i\Psi_i$. The diffusion map after τ time steps $\Psi_\tau: X \to R^\omega$ embeds each node i = 1, . . . , n in the Markov chain into a ω dimensional Euclidean space where the clustering of the datapoints can be done using k-means

$$i \to \Psi_\tau(i) = \begin{pmatrix} \lambda_1{}^\tau\Psi_1(i) \\ \lambda_2{}^\tau\Psi_2(i) \\ \vdots \\ \lambda_\omega{}^\tau\Psi_\omega(i) \end{pmatrix} \quad (4)$$

A common choice for the kernel k(.,.) is the Gaussian kernel, i.e. $k(x,y) = \exp\left(-\frac{d^2(x,y)}{2\sigma^2}\right)$, where d is a distance over the set X and σ a scale factor. To present an intuitive explanation, we can say that a row normalized Markov matrix (p) is the time domain representative of the graph and the scaled eigen functions $\Psi_\tau(i)$ play the role of Frequency domain coefficients, clustering of which provides the graph partitioning.

3. IMPLEMENTING DIFFUSION MAPS ON GRAYLEVEL IMAGES

In order to apply the diffusion maps to OCT images, graph nodes must be associated with the image pixels. We employ the diffusion map in 2 sequential steps, the first of which segments 5 layers simultaneously, i.e., the 1st, and 7th to 10th layers. Each layer corresponds to a distinct anatomical structure. The second step identifies the inner layers, i.e., 2nd to 6th layers. For implementing the first step, we select 10×10 pixel boxes as graph nodes and the kernel is defined as:

$$k(x,y) = \exp\left(-\frac{d^2(x,y)}{2{\sigma_{geo}}^2}\right).\exp\left(-\frac{d^2(g(x),g(y))}{2{\sigma_{gray}}^2}\right) \quad (5)$$

where x, y indicates the centroids of selected 10×10 boxes, $g(.)$ is the mean gray level of each box, σ_{geo} and σ_{gray} point out the scale factor calculated as .15 times the range of $d(x,y)$ and $d(g(x),g(y))$ respectively. Subsequently, k-means clustering with k=3 is applied to the Euclidean space constructed by eigenfunctions (Fig.1.b). The edge points of the upper and lower clusters are extracted and the results enhanced based on applying the following operators on edges: cubic spline smoothing, local regression using weighted linear least squares, and 2nd degree polynomial models. In the next step, the extracted edges are moved to the lowest vertical gradient in a vertical search area of 10 pixels above and 10 pixels below. 1st and 7th layers were obtained in this step and the 8th – 10th layers were detected by looking for the highest and lowest (alternatively) vertical gradients in a vertical search area of 10 pixels below (Fig. 2. a). The unwanted drift of the OCT images is then removed according to 9th layer to change each column of image in order to produce a linear layer in the place of the 9th section (Fig.2.b).

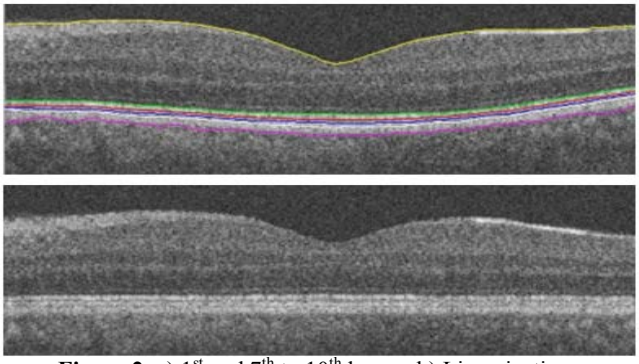

Figure.2. a) 1st and 7th to 10th layers, b) Linearization.

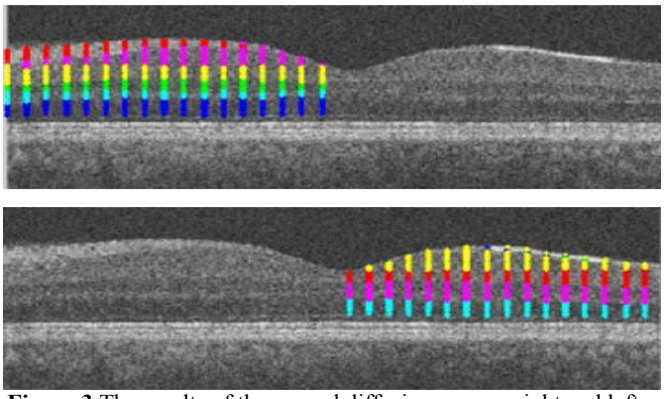

Figure.3.The results of the second diffusion map on right and left parts of the image.

In the next step, the pixel boxes representing the graph nodes are selected as very thin horizontal rectangles $(2 \times 20\ pixels)$. This selection is according to the structure of OCT images after linearization (Fig.2.b). The kernel is selected similar to (5) and the k-means clustering is applied with k=5. The area of image was divided in two (right and left) parts to increase the accuracy of the method (Fig. 3). It should be mentioned that in the case of overall assessment of the images (without breaking to right and left parts), the algorithm couldn't find proper subgroups. For instance, the first layer in right and left part of figure 3 has no connections and couldn't be merged to form a good cluster in diffusion map algorithm.

The edge points of clusters were then extracted and the points were connected to make a smooth curve. In the final step the curves were connected together to form the final segmentation (Figs. 4 and 5).

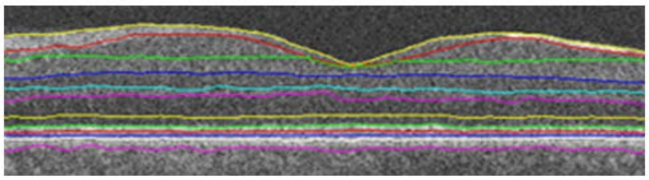

Figure.4. Final segmentation on the aligned image.

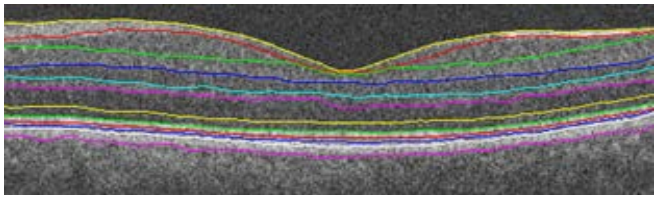

Figure.5. Final segmentation on the original image.

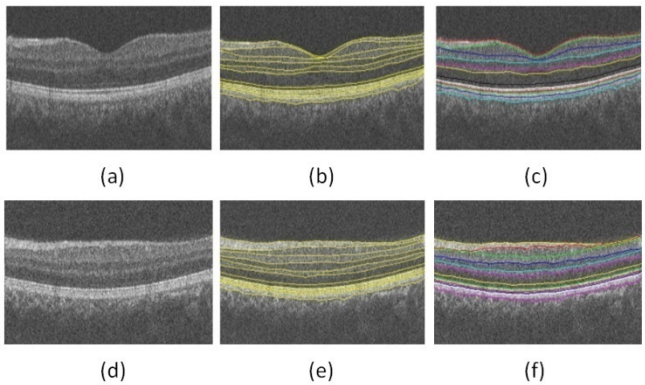

Figure.6. Two example results. (a,d) Composite image. (b,e) Composite image with average manual tracing (c,f) Composite image with segmented borders in 2D.

4. EXPERIMENTS AND RESULTS

The proposed method is tested on thirteen 3D macular SD-OCT images obtained from eyes without pathologies with Topcon 3D OCT-1000 imaging system (with a size of 650 × 512 × 128 voxels and a voxel resolution of 4.81 × 13.67 × 24.41 μm^3). The mean unsigned and signed border positioning errors (mean ± SD) was 8.52±3.13 and -4.61±3.35 micrometers, respectively. Fig.6 shows examples of our segmentation results. Manual segmentation is obtained using mean value of segmentation by two independent observers. The average manual tracing is used

as ground truth to evaluate the method. The mean unsigned and signed border positioning errors for each border are computed and presented in TABLE 1.

The average computation time of the proposed algorithms (implemented with MATLAB) was 12 seconds per 2D slice. We applied the k-means clustering for 100 iterations and selected the clustering result with the highest with-in-class and the lowest between-class index.

The OCT images were segmented to locate all of the 11 proposed layers in [14], furthermore, one extra layer between 6^{th} and 7^{th} layer was located which is named 6a in this paper.

Table 1. Summary of mean unsigned and signed border positioning errors (mean ± sd) in micrometers

Border	mean unsigned errors Avg. Obs. Vs. Alg.	mean unsigned errors Obs. 1 vs. Obs. 2	mean signed errors Avg. Obs. Vs. Alg.	mean signed errors Obs. 1 vs. Obs. 2
1	6.88±3.22	6.25±3.12	4.85±2.42	-5.34±2.31
2	12.82±5.56	15.94±8.94	-13.54±5.65	13.16±6.56
3	10.94±4.13	10.63±6.19	-13.22±4.38	13.37±6.39
4	15.03±5.12	16.25±9.27	-16.23±5.62	13.06±7.24
5	10.05±3.74	12.82±5.36	-7.63±4.21	9.84±5.21
6	13.75±3.18	12.53±4.89	-11.34±5.34	12.88±6.13
6a	6.57±2.13	7.81±3.76	6.62±1.21	-12.28±2.36
7	3.44±1.01	5.63±2.23	3.16±1.24	-6.06±2.34
8	4.07±2.08	5.61±2.58	3.97±2.12	5.91±1.54
9	5.05±1.29	8.42±3.95	-3.91±1.65	7.09±2.18
10	6.25±2.37	6.55±3.84	-4.16±2.37	7.31±1.94
11	6.88±2.42	7.19±2.45	-3.60±2.46	8.97±2.94
overall	8.52±3.13	9.65±4.83	-4.61±3.35	5.71±3.98

5. CONCLUSION

This research shows the ability of diffusion maps in segmentation of gray-level images for the first time. As it could be found in section 1, diffusion map has a wide range of application in medical image segmentation [15-18]. However, the under investigation images were all corresponding to high dimensionality of each pixel (or voxel) like diffusion MRI or fMRI and higher spectral microscopic images. But, our OCT images are simple gray leveled pixels (or voxels). However, two important points should be considered:

A. Every algorithm capable of dealing with high dimensionality of points, is able to handle the low dimensional (and even one-dimensional) datasets.

B. In order to reduce the effect of unavoidable noise of OCT images and to get rid of very complicated and time consuming noise reduction in preprocessing step, we may select more than one pixel (or voxel) as the nodes of our graph and select three categories of textural features (Statistics, Co-occurrence Matrix, Run-Length Matrix) from each node to measure the similarity between the nodes.

6. RELATION TO PRIOR WORK

The proposed method is obviously categorized in 3D graph based methods, but the graph partitioning was usually based on properties in the graph domain like gradient or texture. But newly developed methods in frequency domain are based on signal analysis in new domains (similar to Fourier transform in signal processing). The proposed Diffusion Map method is similarly working on Fourier transform applied on graphs and the method can utilize the intrinsic capabilities of the frequency space consequently. In contrast to recent methods of graph based OCT image segmentation [12, 14], the presented approach does not require edge-based image information and rather relies on regional image texture through space-frequency analysis [15, 19]. Consequently, the proposed method demonstrates robustness in situations of low image contrast or poor layer-to-layer image gradients.

7. ACKNOWLEDGMENT

This work was supported in part by the National Institutes of Health grants R01 EY018853, R01 EY019112, and R01 EB004640

8. REFERENCES

[1] Huang, D., Swanson, EA., Lin, CP., Schuman, JS., Stinson, GW., Chang, W., Hee, MR., Flotte,T., Gregory, K., Puliafito, CA. and Fujimoto JG. “Optical coherence tomography”. Science 254, 1178–81 ,1991.

[2] Delia Cabrera DeBuc, A Review of Algorithms for Segmentationof Retinal Image Data Using OpticalCoherence Tomography, Image Segmentation, InTech, 2010.

[3] Hee, MR., Izatt, JA., Swanson, EA., Huang, D., Schuman, JS., Lin, CP., Puliafito, CA. and Fujimoto, JG. “Optical coherence tomography of the human retina”. Arch. Ophthalmol. 113, 325-32, 1995.

[4] George, A., Dillenseger, JA., Weber, A. andPechereau, A. (2000). Optical coherence tomography image processing.Investigat.Ophthalmol.Vis.Sci., vol. 41, pp. S173–S173

[5] Koozekanani, D., Boyer, KL.,Roberts, C. (2001). Retinal Thickness Measurements in Optical Coherence Tomography Using a Markov Boundary Model. Medical Imaging, IEEE Transactions on 20(9), 900–916

[6] Boyer, KL., Herzog, A., Roberts, C. (2006). Automatic recovery of the optic nervehead geometry in optical coherence tomography.IEEE Trans Med Imaging.May; 25(5):553-70. PubMed PMID: 16689260.

[7] Baroni, M., Fortunato, P. and Torre, AL. (2007). Towards quantitative analysis of retinal features in optical coherence tomography. Medical Engineering and Physics 29(4), 432–441

[8] Cabrera Fernández, D., Villate, N., Puliafito, CA. and Rosenfeld, PJ. (2004). Comparing total macular volume changes measured by Optical Coherence Tomography with retinal lesion volume estimated by active contours. Invest. Ophthalmol. Vis. Sci. 45: E-Abstract 3072.

[9] Yazdanpanah, A., Hamarneh, G., Smith, B., Sarunic, M. (2009).Intra-retinal layer segmentation in optical coherence tomography using an active contour approach.Med Image ComputComput Assist Interv. 12(Pt 2):649-56.

[10] Fuller, AR., Zawadzki, RJ., Choi, S., Wiley, DF., Werner, JS. andHamann, B. (2007).Segmentation of Threedimensional Retinal Image Data. IEEE Transactions on Visualization and Computer Graphics 13(6), 1719–1726

[11] Mayer, MA., Tornow, RP., Bock, R., Hornegger, J. and Kruse, FE. Automatic Nerve Fiber Layer Segmentation and Geometry Correction on Spectral Domain OCT Images Using Fuzzy C-Means Clustering. *Invest. Ophthalmol. Vis. Sci.* 49: E-Abstract 1880. 2008.

[12] Abràmoff, MD., Lee, K., Niemeijer, Wallace, L., Alward, M., Greenlee, EC., Garvin, MK., Sonka, M. and Kwon, YH. "Automated Segmentation of the Cup and Rim from Spectral Domain OCT of the Optic Nerve Head." Invest. Ophthalmol. Vis. Sci. 2009 50: 5778-5784, 2009.

[13] Lee, K., Abramoff, MD., Niemeijer, M., Garvin, MK., Sonka, M. "3-D segmentation of retinal blood vessels in spectral-domain OCT volumes of the optic nerve head." Proc. of SPIE Medical Imaging: Biomedical Applications in Molecular, Structural, and Functional Imaging, vol. 7626, p. 76260V, 2010

[14]Quellec, G., Lee, K., Dolejsi, M., Garvin, MK., Abràmoff, MD. and Sonka, M. Three-dimensional analysis of retinal layer texture: identification of fluid-filled regions in SD-OCT of the macula. IEEE Trans. Med. Imaging. 29(6), pp.1321–1330, 2010.

[15] Joel Andersson, Diffusion Geometry with Applications to Virus Classification, Master thesis, 2008

[16] Xilin Shen, Franc¸ois G. Meyer. Nonlinear dimension reduction and activation detection for fMRI dataset. Proc. Of conf. on Computer Vision and Pattern Recognition Workshop.2006.

[17] D Wassermann, M Descoteaux, R Deriche, Diffusion Maps Segmentation of Magnetic Resonance Q-Ball Imaging. Journal of Biomedical Imaging - Recent Advances in Neuroimaging Methodology, 2008.

[18] R. Neji, G.Langs, Unsupervised classification of skeletal fibers using diffusion maps, IEEE International Symposium on Biomedical Imaging: From Nano to Macro, 2009. ISBI '09., 2009

[19] R.R. Coifman, S. Lafon, "Diffusion maps," Applied and Computational Harmonic Analysis 21 (1) 5–30. 2006.